CHAPTER 108

The Pressure Field due to Steep Water Waves Incident on a Vertical Wall

D.H.Peregrine[1] & M.E.Topliss[2]

Abstract

The entrained air present when a wave impacts upon a vertical wall is modelled. A numerical boundary-integral method is applied, with appropriate initial conditions giving a prescribed surface profile and corresponding velocity potential, to model an overturning wave trapping a single air pocket between the oncoming wave front and the vertical wall. The resulting detailed computations provide suitable initial parameters for a simple theoretical model of the trapped air pocket as described in Topliss, Cooker & Peregrine (1992). The fundamental frequencies, and pressures on the impact wall due to the bubble can thus be estimated from the numerical computations. Video frames of small-scale experiments by Hattori & Arami (1992 and private communications) are also examined in detail and similar use of the model provides further pressure estimates. The resulting frequencies and maximum pressures are compared with the measured values. The peak pressures on the impact wall are within 30% of those measured and the frequencies are generally closer. Scaling with wave size is also discussed.

Introduction

Much attention has been given to the peak pressures developed when storm waves meet sea walls and breakwaters, e.g. experimental studies by Kirkgöz (1991), Hattori & Arami (1992), Oumeraci & Partenscky (1992) and theoretical studies by Cooker & Peregrine (1990,1992). These breaking-wave impacts can

[1]Professor of Applied Mathematics, School of Mathematics, Bristol University, University Walk, Bristol BS8 1TW, England. (*d.h.peregrine@bristol.ac.uk*)

[2]Research Student

have substantial aeration, either as air trapped at the wall or as pre-entrained air.

Aeration in wave impacts has been described in the laboratory experiments as either a cloud of small air bubbles in the water adjacent to the vertical structure or as a single air pocket trapped between the overturning wave and the impact wall. Numerical computations presented in this paper can simulate the motion of an overturning wave against a vertical structure on a finite depth, up until point of impact. This provides detailed data which can be used with theoretical analysis to describe the initial motion of an air pocket. Comparison of the analytic theory with the computations and experimental data, in particular that of Hattori & Arami (1992 and private communications) and Hattori, Arami & Yui (1994), has led to fairly good agreement with the various parameters. Three experimental data sets have been compared with computations that produce the same size air pockets.

The majority of experiments undertaken to study wave impact are performed in small-scale tanks and a discussion of scaling from model to prototype completes the paper.

Numerical Method

The numerical method used in this paper for computing the unsteady two-dimensional motion of a water surface, including that for breaking waves, is described in Dold & Peregrine (1986) and Dold (1992).

The fluid is taken to be incompressible and the flow irrotational so that a velocity potential can be defined such that $\mathbf{u} = \nabla\phi$ and ϕ satisfies Laplace's equation with the fully nonlinear free surface boundary conditions.We have taken the pressure immediately above the free surface to be a constant and neglected surface tension.

The surface profile and velocity potential are prescribed on the free surface as initial data. The domain is reflected about the bed $y = -h$ to form a symmetric image flow where a point on the upper free surface has an image on a lower free surface. The free surface boundary conditions are satisfied at the free surface which moves with time. The surface of the fluid is considered to be a smooth continuous profile approximated by a set of discrete points. A truncated Taylor series is used to perform explicit time-stepping. Cauchy's integral theorem is used to obtain a boundary integral equation for the evaluation of velocities and multiple derivatives of the surface motion. After the unsteady surface motion is calculated, the velocity and pressure beneath the surface can be evaluated at points over a rectangular grid. Variables are scaled accordingly: $y^* = y/h$, $x^* = x/h$, $p^* = p/\rho gh$, $t^* = t\sqrt{g/h}$, $u^* = u/\sqrt{gh}$ and $A^* = Ag$ where h is a chosen value and $*$ represents the scaled variables.

Computations for an overturning 'tanh' wave.

Using this boundary-integral method for a non-periodic surface, Cooker (1990) has described the motion of a wave overturning immediately before a vertical wall (with a finite depth), trapping a pocket of air against the wall. This was achieved by allowing two equal waves propagating in opposite directions towards each other to form a flow which is symmetric about a point. This is equivalent to a single wave approaching a vertical wall at this point. The initial data used obtained from a tanh expression describing a long wave of elevation:

$$u(x) = -\frac{1}{2}u_o \left\{ 1 + \tanh\left[\frac{(x - x_o)}{s} \right] \right\} \tag{1}$$

where x_o is the initial centre of the wave, u_o is the initial maximum velocity, and s is a constant. The wave elevation is of the form $\eta(x) = |u| + \frac{1}{4}u^2$ which gives a wave propagating towards the wall by shallow water theory. This long shallow water wave steepens and breaks as it propagates into water of constant depth, for an example see the surface profiles in figure 1. The computations have to stop just before the wave jet comes into contact with the wall and so the results only describe the motion immediately before impact.

Three examples have been studied of a wave overturning immediately in front of a vertical wall. Different initial positions of the wave give different size air pockets to illustrate the varying characteristics of the motion due to the volume of air trapped. In this section, h is the lowest water depth at the wall. Approximately 250-350 discretisation points were used for the surface of the wave. The wave is taken to have a large initial amplitude of 1.7 with $s = 2.0$, chosen to obtain large air pockets. Accuracy tests with more discretisation points have been very satisfactory. Surface profiles are presented for several timesteps and the pressure contours below the free surface have been evaluated in each case for the final computed time.

The first example (example 1) presented has an initial distance from the wall of $x_o = 8.0$.

The wave steepens and begins to overturn as it comes nearer to the wall as portrayed in the time history of the surface profiles in figure 1. The timesteps are reduced as the wave becomes steeper and the motion more violent. The computations stop just before impact with a small pocket of air is trapped between the wave front and the wall.

The pressure field at the final computed time shown in figure 2 has pressure contours in increments of 0.4. The thickened line represents the water surface. As well as high pressures at the foot of the wall, a region of much higher pressure is found just below the waterline with very tightly packed contour lines. Note that no direct impact between the water and the wall has yet occured. The high pressures are spread over a substantial area of the fluid domain.

For a similar wave of amplitude 1.7, the initial distance of wave from wall

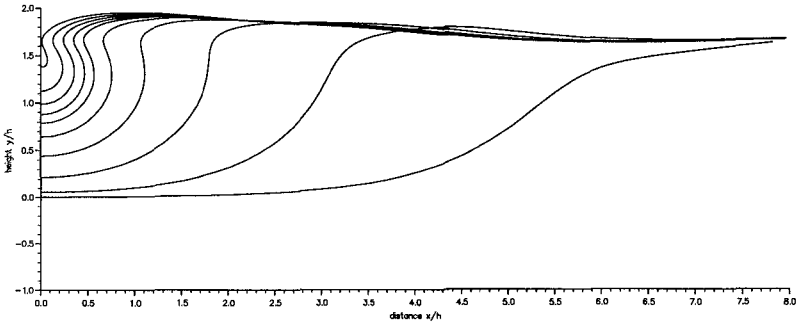

Figure 1: Surface profiles for a tanh waveform of amplitude 1.7, initial distance 8.0 at times 1.53, 2.81, 3.45, 3.77, 3.93 and 4.01 - 4.17 in steps of 0.04.

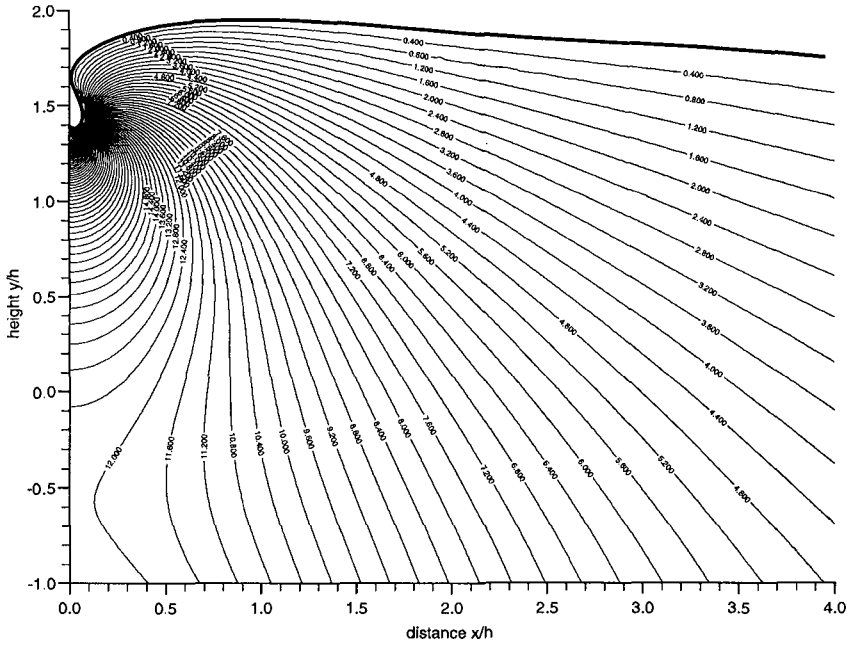

Figure 2: Pressure contours for a tanh waveform of amplitude 1.7, initial distance 8.0 at time 4.17 with increments of 0.4.

is now increased to $x_o = 9.0$ in example 2. The time history of the surface profiles of the wave is displayed in figure 3. The waterline at the wall now lower and a larger amount of air is trapped. As can be seen in figure 4, the isobars, are at the same intervals, and show much lower pressures and pressure gradients than in example 1. Now the greatest pressures are at the bed.

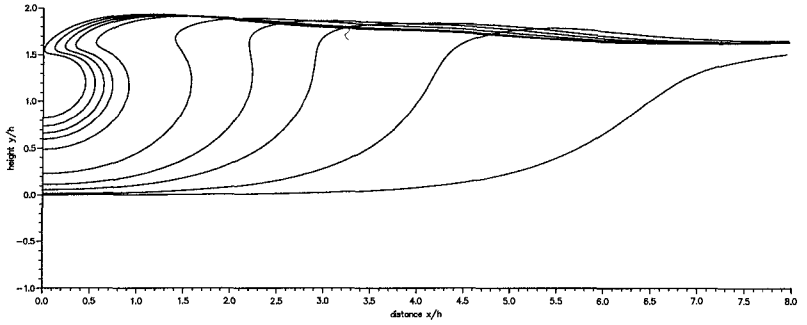

Figure 3: Surface profiles for a tanh waveform of amplitude 1.7, initial distance 9.0 at times 1.48, 2.76, 3.40, 3.72, 4.04, 4.36 and 4.44 - 4.56 in steps of 0.04.

Example 3 has a further increase of initial distance of the wave from wall to $x_o = 10.0$. The wave now overturns further from the wall and produces the largest air pocket. The surface profiles in figure 5 show the time history of the wave. Figure 6 shows the pressure distribution under the free surface for the final profile before impact has lower values than for the previous two examples. The pressure field is now in sharp contrast with the pressures of example 1, as the isobars are almost horizontal, indicating that pressures are not much in excess of hydrostatic. These three examples show that as the amount of air trapped increases, the pressures decrease and the characteristics of the pressure field change. Other examples have confirmed this trend.

The numerical data from the final computed times enables the characteristics of the three examples to be studied and compared. A representative set of numerical data includes the incident wave amplitude be H_o, the vertical height of the water above the bed after the final computational time be H, the vertical height of the water line in contact with the wall at the final computed time be H_w, and the vertical velocity, acceleration at this point be u_p, a_p respectively as shown in figure 7. The initial wave amplitude H_o is 1.7 in all three cases, but with three different size air pockets resulting from the original placing of the wave with regard to the wall. Let the horizontal velocity at the centre line of

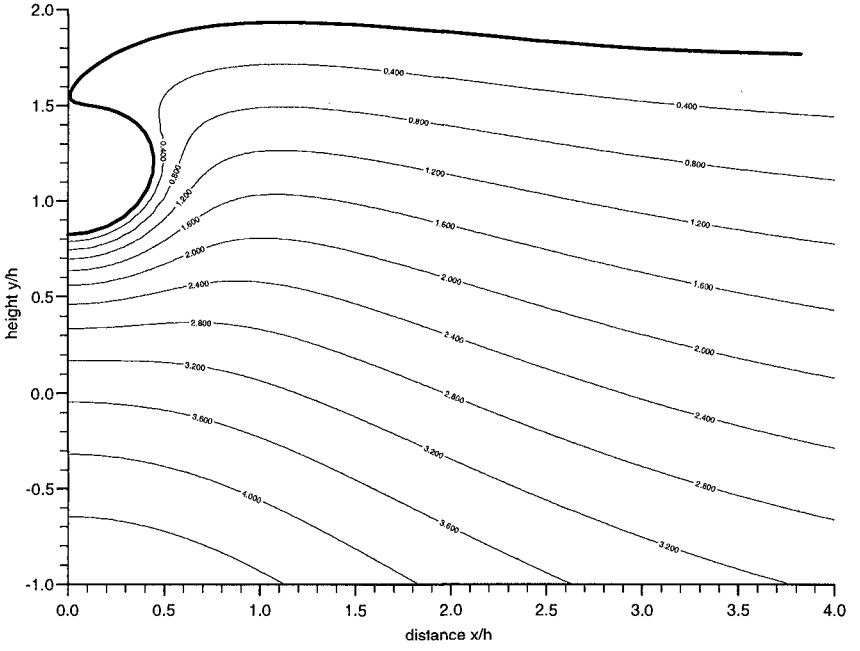

Figure 4: Pressure contours for a tanh waveform of amplitude 1.7, initial distance 9.0 at time 4.56 with increments of 0.4.

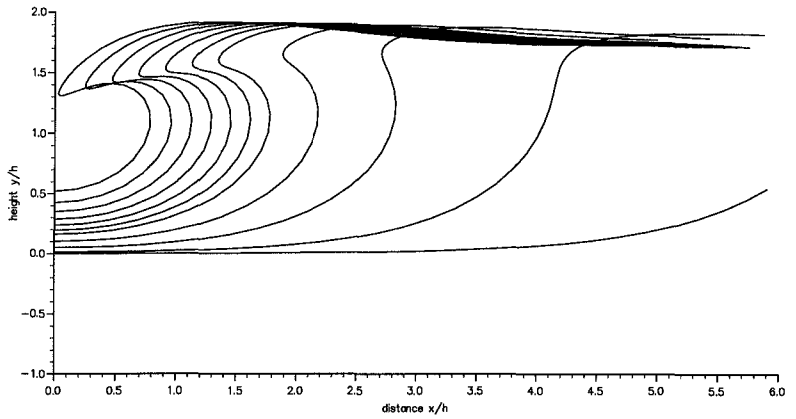

Figure 5: Surface profiles for a tanh waveform of amplitude 1.7, initial distance 10.0 at times 2.0, 3.28, 3.92, 4.24 and 4.44 - 4.92 at steps of 0.04.

the pocket be u_f and the horizontal velocity at the tip of the jet be u_t. The respective parameters for the three examples from the numerical results of the final computed time are shown in table 1. The horizontal velocity at the centre line of the bubble becomes much smaller as the radius of the pocket increases with the horizontal velocity of the tip of the jet not significantly altered. Thus in the first two examples, the velocity of the jet tip is larger than the velocity of the centreline as noted by Hattori, Arami & Yui (1994). In addition the upward velocity of the waterline at the wall decreases rapidly with the formation of larger pockets leading to the forward velocity u_f becoming greater than the upward velocity u_p.

For very small bubble sizes, large values are obtained for the vertical velocity and acceleration of the waterline. This shows an approach to the violent conditions reported by Cooker & Peregrine (1990) in their report of the "flip through" phenomenon. The vertical height of the waterline at the wall becomes much lower as the amount of air trapped increases resulting in the ratio H_w/H becoming smaller. These ratios are in agreement with those presented by Oumeraci, Klammer & Partenscky (1993).

Comparison of numerical and experimental data

The numerical method for an overturning wave provides many parameters allowing different sizes of air pockets to be studied. Given experimental results,

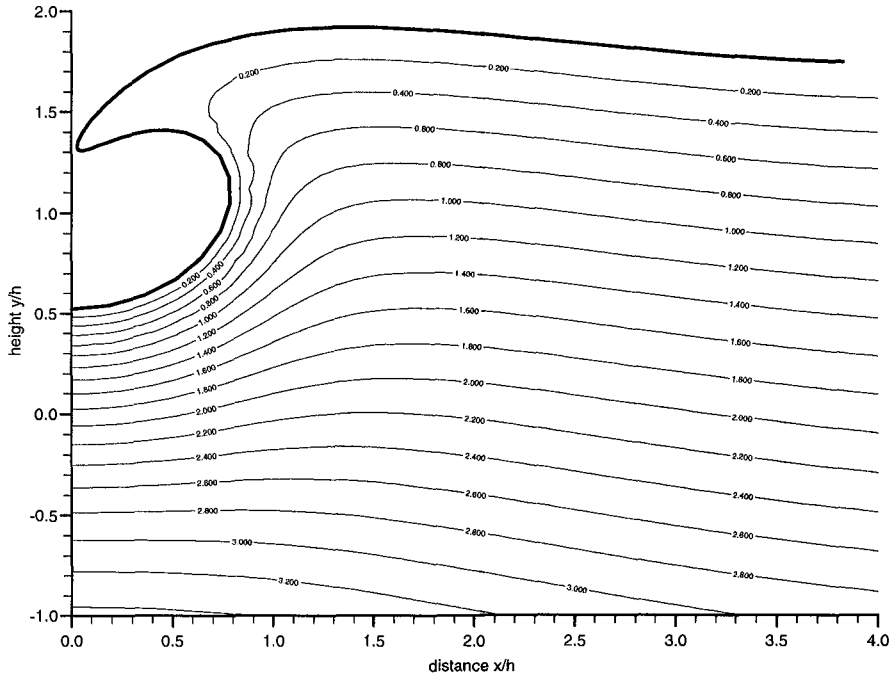

Figure 6: Pressure contours for a tanh waveform of amplitude 1.7, initial distance 10.0 at time 4.92 with increments of 0.2.

	Example 1	Example 2	Example 3
Wave amplitude H_o	1.7	1.7	1.7
Initial distance from wall	8.0	9.0	10.0
Pocket radius	0.071	0.445	0.784
Vertical height H	2.75	2.85	2.84
Vertical height H_w	2.390	1.823	1.522
Vertical velocity u_p	15.821	2.368	1.345
Vertical acceleration a_p	1700.7	10.93	4.09
Horizontal velocity u_f	5.35	2.69	1.99
Horizontal velocity u_t	3.06	2.81	2.77
Ratio H_w/H	0.869	0.640	0.536

Table 1: Comparison of dimensionless numerical data from the final computed times for the three tanh waveform examples.

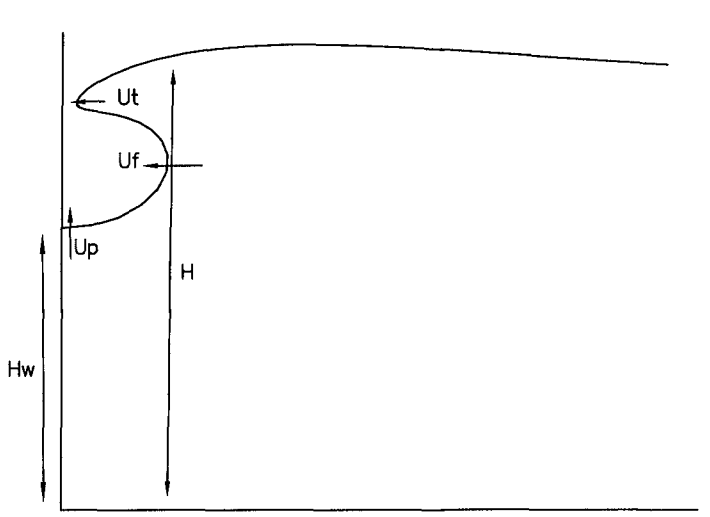

Figure 7: Parameters for an overturning wave

either with data showing the size of a trapped air pocket and its position under the free surface or photographs from which these parameters can be measured, a computation can be used to model the overturning wave by producing a resulting trapped air pocket of the same dimensions. We choose a computation to compare with an individual experiment by varying the initial wave height H_o and distance from the wall x_o until the computation gave a trapped air pocket which was a good match with the values for the radius r, the distance d of the bubble centre from the bed and the height H of the water after impact measured from the experimental data. We have compared with video frames from Hattori & Arami (1992). For a bubble nearer the bed than the free surface, a higher incident wave amplitude is required to obtain a correct d/H ratio. For a larger bubble, the initial distance of the wave from the wall needs to be increased as shown in the above examples. The numerical data for the final computed time gives values for the normal velocities around the curved surface which can then be averaged to give a radial velocity u_r.

The subsequent motion of the trapped air pocket has been modelled as a two-dimensional semi-circular bubble using Topliss, Cooker & Peregrine's (1992) result for the fundamental frequency. To a first approximation, it is

$$\omega^2 = -\frac{2\gamma p_o}{\rho_l a^2 \log[\frac{1}{4}(\pi a/H)\,\tan(\frac{1}{2}(\pi d/H))]} \tag{2}$$

where ρ_l is the density of water, p_o the atmospheric pressure, γ the ratio of specific heats and $\omega = 2\pi f$ where f is the fundamental frequency of the bubble. Once values for a, d, H and u_r have been obtained, either from a computation or, as in the next section, from experimental measurements, the frequencies and amplitudes of oscillation of the bubble can be predicted using equation 2, the linearised kinematic boundary condition, $u_r = \omega\epsilon_o$, $\alpha_o = a\epsilon_o\omega$ and the corresponding expression for maximum pressure,

$$p_{max} = -\rho\omega\alpha_o \log\left(\frac{\lambda a}{2}\tan(\lambda d)\right) \tag{3}$$

Hattori & Arami have provided us with many details of their experiments to investigate the importance of a trapped air pocket between the breaking wave and the wall. The experiments were undertaken in a small wave tank with a 1:20 bed slope to cause the wave to break. In each case the still water depth was five centimetres. High-speed video frames were taken of the fluid motion with simultaneous pressure histories. The experimental data sets with large clear trapped air pockets were chosen for comparison.

The histories of the pressure, measured on the impact wall immediately after impact exhibit three stages when air is trapped. Initially the pressure rises to a peak value and is followed by an interval of regular smooth oscillations, of decreasing amplitude. These oscillations are displayed with the same frequency in all six pressure gauges. This finally develops into a more confused signal, consisting of higher frequencies with lower amplitudes, and which carries on for an indefinite time.

The photographs show a cylindrical air pocket trapped between the wave front and the structure immediately after impact. In the video frames following the impact, it can be seen that the free surface rises and a thin jet of water shoots up the wall. We neglect this since it is usually much thinner than the bubble until a later stage and assume a flat surface in our models. The damped oscillations recorded by Hattori & Arami decay exponentially like $e^{-\beta t}$. The peak pressure is presented in the dimensionless form $p^* = p/\rho g H_o$ where H_o is the incident wave height above the bed.

Three sets of experimental data on the formation of an air pocket by Hattori & Arami have been examined in detail. In each case measurements have been taken from the video frames to obtain values for a, d, H, u_f, where u_f is the forward velocity as previously defined. The bubble surface in the frames is not sufficiently well defined to take measurements around the surface and so the value obtained for u_f is used for the average radial velocity u_r. The video frames indicate a horizontal free upper surface at impact and so the computations of a tanh waveform should provide a good numerical model. For each of the cases studied, a table below shows the values of a, d, H and u_r obtained from both measuring the video frames of the experiments and from the corresponding computation The table also gives the *estimated* values of f, ϵ_o, α_o and maximum

p^* using the theoretical analysis for a semi-circular bubble and the measured values of peak pressure and oscillation frequency.

In experiment No. 132-3 the bubble radius was measured to be 7.5 mm from the video frames. Comparisons are made with a computation using a wave of initial dimensionless amplitude 8.0 and at an initial distance 6.5 from the impact wall. The corresponding dimensional value is 72 mm for wave height and there are comparable values for d and H. The radial velocity given by the numerical computations also gives agreement with that measured from the photographs. The top line in the table gives the maximum experimentally measured pressure and the frequency of its oscillation.

	d	H	f	u_r	ϵ_o	α_o	p^*
Hattori & Arami			190				38.1
From video	0.0295	0.066	221	1.0	0.00072	0.0075	43.5
Computation	0.0219	0.055	222.2	0.95	0.00068	0.0070	35.4

Table 2: Comparison of theory with experiment and computation for a pocket of radius 7.5 mm.

In experiment No. 172-3 the trapped air pocket, from the video frames, had radius 9.5mm. The computation producing a trapped pocket of the same size uses a wave of initial dimensionless height 5.0 and initial distance of 7.4, corresponding to 62 mm dimensional wave height .

	d	H	f	u_r	ϵ_o	α_o	p^*
Hattori & Arami			210				55.7
From video	0.029	0.063	186.5	1.1	0.00093	0.01	49.0
Computation	0.03	0.061	191.5	0.99	0.00082	0.0094	39.7

Table 3: Comparison of theory with experiment and computation for pocket of radius 9.5 mm.

The third data set, experiment No. 178-3, has the largest trapped air pocket, radius 20 mm, and produces the lowest pressures. The computation of initial dimensionless wave amplitude 7.0 with an initial distance from the impact wall of 9.0 corresponds to an incident wave height of 86 mm.

As can be seen from the comparisons, reasonable agreement is obtained between the experimental and theoretical results with larger bubble sizes producing lower frequencies. The measurements from the frames show that the lower surface rises more rapidly up the wall for a smaller pocket in agreement with the numerical computations. The damping of the oscillations appears to

	d	H	f	u_r	ϵ_o	α_o	p^*
Hattori & Arami			106				22.5
From video	0.026	0.067	99	0.8	0.0014	0.015	28.7
Computation	0.029	0.069	101.2	0.76	0.0012	0.015	20.0

Table 4: Comparison of theory with experiment and computation for a pocket of radius 20 mm.

be not as strong for the largest bubble and the oscillations last the longer. The slow rise of the pocket and mass of small bubbles in the video frame during the oscillations indicate little air loss initially through the surface of the water. The damping of pressure oscillations is yet to be modelled.

difference with Hattori & Arami	pressure from video	pressure from computation	frequency from video	frequency from computation
132-3	+12 %	-7 %	+16%	+17%
172-3	-12 %	-29 %	-11%	-9%
178-3	+22 %	-11 %	-7 %	-5%

Table 5: Comparison of the maximum pressure and oscillation frequency estimates for the three data sets.

The pressures predicted by the theory give reasonable agreement for both the experimental and computational parameters. Table 5 shows the differences in the pressures and frequencies estimated compared to those those measured by Hattori & Arami in each of the three experiments. The pressure differences are the percentage change between the peak pressures recorded in the data and the predicted values from the theory. Differences with those from the computations are all lower. The frequencies are generally closer to the experimental values.

Scaling

Most experiments undertaken to investigate wave impact on vertical structures involve laboratory model-scale wave flumes. Scaling from model to prototype remains a complex and not fully understood problem. The number of parameters concerning the motion need to be identified and mathematical relationships established between the dimensionless scaling parameters.

When modelling the entrained air as either a single air pocket or a uniform bubbly mixture, expressions for the resonant frequencies have been obtained in

each case. Peregrine (1994) has suggested, to get order of magnitude estimates, a simpler approximation, similar to

$$\omega = (\gamma g H_a / C)^{1/2} \tag{4}$$

but without γ, where C is the volume of trapped air per unit length of wall (r^2 for a single bubble or LH for a mixture of bubbles in a layer of width L at the wall), H_a is the hydrostatic head of water equal to atmospheric pressure. The comparison of this formula with γ=1.0 (for isothermal bubbles) and 1.4 with the analytical expressions in each case is shown in figure 8. As can be seen

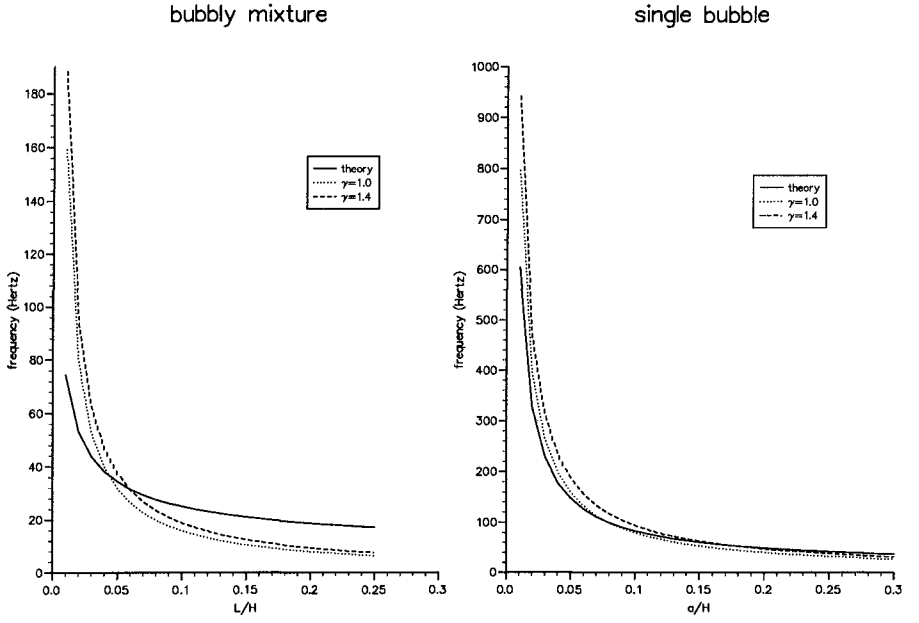

Figure 8: Comparison of the estimated fundamental frequencies, for a single cylindrical bubble with d/H=0.5 (right) and for a column of bubbles next to a wall with α=0.1 (left).

from figure 8, the simplified formula presented by Peregrine is within a factor 2, particularly for the single air bubble, except for small pockets or very thin columns of bubbles.

Peregrine (1994) also presents a simple expression to estimate the maximum pressures:

$$\frac{p_{max}}{\rho g h} = \beta \left(\frac{h H_a}{C} \right)^{1/2} \tag{5}$$

where β is the fraction of the wall over which this impact occurs. For a reasonable ranges of β, 0.1 to 1.0, and C, 0.01 h^2 to 0.25 h^2, this gives

$$0.2\left(\frac{H_a}{h}\right)^{1/2} \leq \left(\frac{p_{max}}{\rho g h}\right) \leq 10\left(\frac{H_a}{h}\right)^{1/2}. \tag{6}$$

To assess these formulas, the maximum pressures for the three experimental data sets studied in have been evaluated using equation (5) with the data taken from the computational parameters and compared with the results obtained previously in tables 2, 3 and 4.

	C	h	β	f	f	p^*	p^*
	m^2	m		eq(2)	eq(4)	eq(3)	eq(5)
No 132-3	$(0.0075)^2$	0.072	0.27	222.2	212.2	35.4	30.8
No 172-3	$(0.0095)^2$	0.062	0.31	191.5	167.5	39.7	25.8
No 178-3	$(0.02)^2$	0.086	0.58	101.2	79.6	20.0	26.9

Table 6: Comparison of estimated frequencies and pressures evaluated earlier for the data sets from Hattori et. al. using the computational parameters, and the simple estimates for frequencies and maximum pressures given by Peregrine.

The maximum pressures predicted by equation (5) show agreement with those predicted by equation (3) to within 30 percent and thus this equation gives a very simple calculation for rough estimates. Looking at the range for the pressures given by equation (5), the values C= 0.01, 0.02 and $0.05h^2$ are obtained for No 132-3, 172-3 and 178-3 respectively, giving $p_{max}/\rho g h$ to be 3.2, 4.4 and 2.1 $(H_a/h)^{1/2}$ respectively, well within in the range given by (6).

References

COOKER, M.J. & PEREGRINE, D.H. (1990) Violent water motion at breaking wave impact. *Proc. 22nd Coastal Eng. Conf. A.S.C.E* Delft pp 1473-1486

COOKER, M.J. & PEREGRINE, D.H. (1992) Wave impact pressure and its effect upon bodies lying on the sea bed. *Coastal Eng.* **18** pp 205-229

DOLD J.W. (1992) An efficient surface-integral algorithm applied to unsteady gravity waves. J. Comp. Phys. 103, 90-115.

DOLD, J.W. & PEREGRINE, D.H. (1986) An efficient boundary-integral method for steep unsteady water waves. in Numerical Methods for Fluid Dynamics II (Eds. K.W.Morton & M.J.Baines), Oxford University Press. pp671-679.

HATTORI, M. & ARAMI, A. (1992) Impact breaking wave pressures on vertical walls. *Proc. 23rd Coastal Eng. Conf. A.S.C.E.* Venice pp 1785-1798
HATTORI, M., ARAMI, A. & YUI, T. (1994) Wave impact pressure on vertical walls under breaking waves of various types. *Coastal Eng.***22** pp 79-114
KIRKGÖZ, M.S. (1991) Impact pressure of breaking waves on vertical and sloping walls. *Ocean Eng.***18** pp 45-59
PEREGRINE, D.H. (1994) Pressure on breakwater: A forward look. *Int. Workshop on Wave Barriers in Deep Water.* Port & Harbour Res. Inst., Yokuska, 553-573
SCHMIDT, R., OUMERACI, H. & PARTENSCKY, H.-W. (1992) Impact loads induced by plunging breakers on vertical structures. *Proc. 23rd Coastal Eng. Conf. A.S.C.E.* Venice pp 1545-1558
TOPLISS, M.E., COOKER, M.J. & PEREGRINE, D.H. (1992) Pressure oscillations during wave impact on vertical walls. *Proc. 23rd Coastal Eng. Conf. A.S.C.E.* Venice pp 1639-1650